JOURNAL OF GEOPHYSICAL RESEARCH, VOL. 99, NO. B4, PAGES 7103–7119, APRIL 10, 1994

The evolution of deformation and topography of high elevated plateaus 1. Model, numerical analysis, and general results

Shimon Wdowinski[1] and Yehuda Bock

Scripps Institution of Oceanography, La Jolla, California

Abstract. A temperature dependent viscoplastic flow model of continental lithosphere is used to investigate the evolution of deformation and topography of high elevated plateaus. Such plateaus are products of both continent-continent collision (Tibetan Plateau) and ocean-continent collision (the Altiplano) and develop in the overriding continental plate. In this study we emphasize the mechanically simpler case of oceanic collision, because it does not involve mass transfer between the two plates. The lithosphere is deformed in response to tectonic and buoyancy forces. The tectonic forces arise from subduction of an oceanic plate (or underthrusting of continental lithosphere) that horizontally indents and vertically shears the overriding lithosphere. The buoyancy forces arise in response to horizontal density variations and tend to relax existing topography or thick crust. The time evolution of the deformation and topography is investigated using a finite element technique that solves for the flow field in the overriding lithosphere. The model produces dynamically supported near-trench topography and inland mountain topography that is isostatically supported by a thick crust. A finite region of localized deformation, thick crust, and high topography develops only if the model includes a horizontal thermal perturbation or an initially thick crust; however, only thermally perturbed lithosphere generates a plateau topography. The shape and size of the calculated plateau depend on the wavelength of the thermal perturbation, Grashof number, and density contrast between the crust and mantle. The time evolution of the deformation shows a significant change in the deformation pattern as the high elevated plateau evolves. During early stages, compressional deformation of the crust and mantle are localized in the thermally perturbed weak zone. At later stages, as the crust thickens, buoyancy forces of larger magnitude resist further thickening of the crust and the locus of compressional crustal deformation migrates inland. This migration does not affect the location of the mantle deformation, which remains in the thermally weak region, but it is accompanied by a significant shear deformation in the weak lower crust. The separation of the crustal locus from the mantle locus of deformation emphasizes the importance of vertically dependent deformation in the formation of high elevated plateaus. This demonstrates the limitations of models that ignore changes of deformation with depth, such as plane stress or thin sheet models.

Introduction

High elevated plateaus form some of the largest morphologic features on Earth's surface, extending over 500,000 km^2 at a mean elevation exceeding 4-5 km above sea level. Their topography is mostly isostatically supported by thick crustal roots and is generally characterized by low relief. At present, only two such plateaus are tectonically active: the Tibetan Plateau and the Altiplano of the central Andes. Both of these are located on the overriding plate in major convergence zones. In addition, geologic studies suggest that similar morphologic structures existed in the past, such as in the western part of North America during the Mesozoic Laramide Orogeny [*Hamilton*, 1969; *Burchfiel and Davis*, 1975]. Understanding the formation and evolution of such plateaus is a critical step in understanding large-scale tectonic processes.

In recent years, applied continuum mechanics has successfully explained many aspects of the formation and evolution of elevated plateaus, such as the Tibetan Plateau [e.g., *England and McKenzie*, 1982, 1983; *Vilotte et al.*, 1982, 1986; *Houseman and England*, 1986; *England and Houseman*, 1986, 1989] and the western part of North America [e.g., *Bird*, 1984, 1988, 1989]. Full three-dimensional calculations of continental deformation are limited by computation resources and therefore are capable of solving only simple problems. Therefore most studies of lithospheric deformation assume a two-dimensional approximation. Many studies used thin sheet or plane stress approximations and investigated the horizontal distribution of topography and deformation in these plateaus [e.g., *England and McKenzie*, 1982; *Vilotte et al.*, 1982; *Bird*, 1984]. However, the thin sheet and the plane stress approximations ignore vertical variations of strength and deformation within the continental lithosphere. *Bird* [1989] recognized the importance of vertical rheological and deformation variations within the continental lithosphere and investigated the evolution of the western North American topography by a two-layer model consisting of the upper crust and the uppermost mantle. Although Bird's formulation is computationally more economical than full

[1]Now at the Geological Survey of Israel, Jerusalem.

Paper number 93JB02381.
0148-0227/94/93JB-02381$05.00

three-dimensional calculations, his results suffer from low resolution.

Mountain building processes have been investigated by critical Coulomb wedges [e.g., *Davis et al.*, 1983; *Dahlen and Barr*, 1989], by thin sheet models [e.g., *England and McKenzie*, 1982; *Vilotte et al.*, 1986], and by vertical plane strain models [e.g., *Chery et al.*, 1991; *Koons*, 1987; *Willet et al.*, 1993; *Wdowinski and O'Connell*, 1991]. Vertical plane strain flow models of continental deformation that include temperature dependent elasto-viscoplastic or viscoplastic rheologics have been mostly used to investigate large scale extensional tectonics [e.g., *Bassi*, 1991; *Christinasen*, 1992]. To our knowledge, *Chery et al.* [1991] is the only study that uses temperature dependent elasto-viscoplastic rheology to investigate large scale compressional lithospheric deformation; this method was successfully applied to the Pyrenees mountain belt. In this study, we take an approach similar to that of *Chery et al.* [1991] and use a temperature dependent viscoplastic rheology to investigate the evolution of topography and deformation of high elevated plateaus.

We present a temperature dependent viscoplastic flow model of the evolution of topography and deformation of elevated plateaus, which include vertical deformation, strength, and density variations of the lithosphere. Because the model depends on many parameters, such as thermal structure, material properties, driving forces, and initial configuration, this paper emphasizes the sensitivity of the model to the various parameters. *Wdowinski and Bock* [this issue] present a comparison between the model's results and observations from the central Andes.

Model

We ignore along-strike variations of deformation and use two-dimensional vertical plane strain calculations. This assumption holds as long as the high elevated plateau is dominated by uniform deformation along-strike, such as in the central Andes. Although the present-day deformation of the Tibetan Plateau is dominated by E-W extension, which violates the plane strain assumption, some of our results nevertheless apply to its early history (for regions that are sufficiently far from the collision boundary), when the deformation was predominantly N-S compression.

High elevated plateaus are products of both continent-continent collision (Tibetan Plateau) and ocean-continent collision (the Altiplano). In both cases, the plateau develops in the overriding continental plate. During continental collision, the overriding plate is underthrust by another continental plate, whereas during oceanic collision, the overriding plate is underthrust by a subducting oceanic plate. Because oceanic collision does not involve mass transfer between the two plates, it is mechanically simpler. Here we emphasize oceanic collision and use the term subducting plate rather than underthrusting plate (Figure 1).

Lithospheric deformation is driven by tectonic (surface) and buoyancy (body) forces. Tectonic forces are induced by a subducting plate that shears the overriding plate along the slip layer and horizontally indents the overriding plate inland (Figure 1a). Buoyancy forces arise in response to horizontal density gradients, which change with time as the topography and the crustal structure evolve.

The model consists of a 100-km-thick continental lithosphere that thins toward the trench as it overrides the subducting oceanic lithosphere at an angle θ. The lithosphere

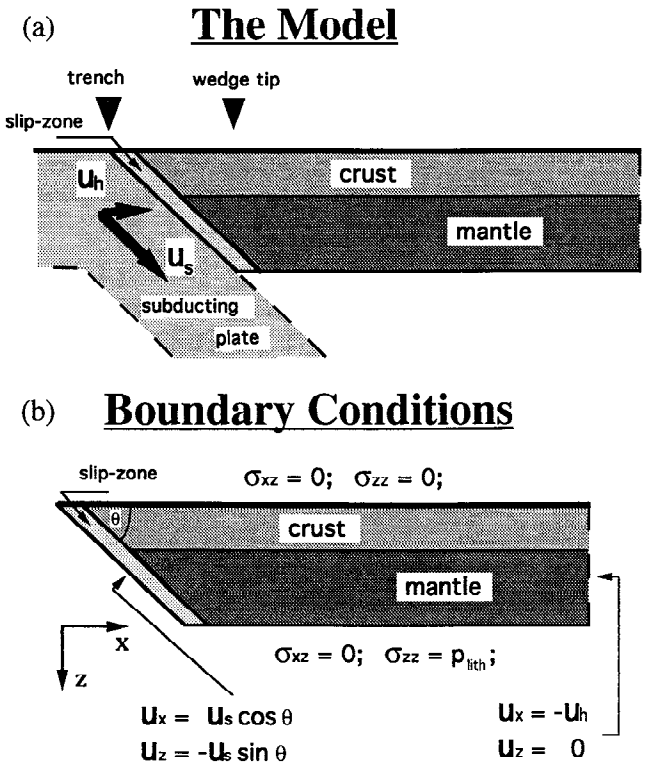

Figure 1. (a) Schematic diagram of the model showing its geometry and the relative plate motion at the subduction boundary. The model consists of a-100-km thick continental lithosphere that is sheared and indented by the subducting plate. The overriding lithosphere is divided into three regions: crust, mantle, and slip layer. The subducting plate and the overriding lithosphere are assumed to converge at a constant rate, which can be described by its direction components parallel to the subduction (u_s) and a horizontal component (u_h). (b) Schematic diagram of the model showing the boundary conditions used in the calculations. The parallel component of the subducting velocity is imposed along the slip layer (u_s), whereas the horizontal component (u_h) is imposed along the other vertical side boundary. θ is the angle of subduction; σ_{xz} and σ_{zz} are components of the stress vector; and p_{lith} is the lithostatic pressure at the base of the lithosphere.

is divided into crust, mantle, and slip layer with different material properties (Figure 1a). As the deformation evolves, the overriding plate shortens as a result of the horizontal indentation by the underthrusting plate. We assume that the lithosphere-asthenosphere boundary remains at depth of 100 km throughout the calculations because below this depth the mantle is sufficiently hot and, therefore, too weak to be considered as lithosphere. Thus material that penetrates below a depth of 100 km is removed from the system. However, we assume that crustal material is conserved resulting in crustal thickening in response to the horizontal shortening. Therefore we do not consider addition or subtraction of crustal material due to accretion, sedimentation, weathering, or tectonic erosion. The subducting and the overriding plates are assumed to converge at a constant rate with a shear component that is parallel to the slip layer (u_s) and a horizontal component (u_h).

The crust and the mantle are assumed to behave as viscoplastic fluids over a geologic timescale. The strength of the lithosphere varies both vertically and horizontally and

depends on material properties, temperature, and stress field. The slip layer represents a narrow region along the contact between the subducting plate and the overriding continental lithosphere that accommodates most of the shear deformation induced by the subducting slab [*Jischke*, 1975; *Wdowinski and O'Connell*, 1991]. It is assumed to be significantly weaker than the crust and the mantle.

Choice of Rheology

The strength of continental lithosphere can be described by four regimes of rock deformation mechanisms: brittle fracture in the crust, ductile flow in the crust, brittle fracture in the mantle, and ductile flow in the mantle [*Brace and Kohlstedt*, 1980]. Brittle failure occurs at low temperatures, when the maximum stress difference between the largest and smallest principle stress axis ($S = |s_1 - s_3|$) reaches the yield stress (τ_y). *Byerlee* [1978] found that frictional resistance of all rock types can be described by a simple linear fit to the normal stress (Byerlee's law). A simplified form of Byerlee's law is given by

$$\tau_y = B\, z \qquad (1)$$

where z is depth and B is a constant that depends on type of failure (normal or thrust) and on the pore pressure. The value of B ranges from 20-60 MPa km^{-1} for compressional failure to 12-25 MPa km^{-1} for extensional failure [*Brace and Kohlstedt*, 1980]; the highest values occur for zero pore pressure.

Ductile flow of rocks occurs at high temperatures due to motion of dislocations in response to deviatoric stresses. Flow in the crust is assumed to be controlled by the strength of quartz, whereas flow in the mantle by the strength of olivine. At the temperature and stress fields of Earth's interior, both quartz and olivine deform by a power law creep [e.g., *Brace and Kohlstedt*, 1980; *Ashby and Verrel*, 1977]. The relation between the deviatoric stress (τ) and the strain rate ($\dot{\varepsilon}$) is given by

$$\tau = \left(\frac{\dot{\varepsilon}}{A}\right)^{1/n} \exp\left\{\frac{Q}{nRT}\right\} \le B\, z \qquad (2)$$

where n is the power law exponent, R is the gas constant, T is the absolute temperature, Q is the activation energy, and A is a constant that depends on the material property. Because the ductile stress cannot exceed the yield stress, the maximum value of the ductile stress is limited by Byerlee's law.

In order to incorporate the brittle and the ductile deformation mechanisms in our model, we adopt a viscoplastic rheology. When the ductile stress is less than the yield stress, the crust and mantle are assumed to behave as incompressible viscous fluids deforming by steady state creep. When the ductile stresses exceed the yield stress, they are assumed to deform plastically ($n \to \infty$). This rheology is represented by the effective viscosity ($\eta_{eff} = \tau/2\dot{\varepsilon}$)

$$\eta_{eff} = \eta_0 \left(\frac{A_0}{A}\right)^{1/n} \left(\frac{\dot{\varepsilon}}{\dot{\varepsilon}_0}\right)^{(1/n - 1)}$$

$$\exp\left\{\frac{Q_0}{nRT_0}\left(\frac{Q/Q_0}{273^\circ/T_0 + T/T_0} - 1\right)\right\} \le \frac{B\, z}{2\dot{\varepsilon}_0}\left(\frac{\dot{\varepsilon}_0}{\dot{\varepsilon}}\right) \qquad (3)$$

where η_0 is a referenced viscosity that is obtained at the referenced strain rate ($\dot{\varepsilon}_0$) and temperature (T_0 in degrees Celsius) for the referenced material properties: activation energy (Q_0) and preexponent (A_0) (Table 1).

Table 1. Values of Constants used in the Calculations

	Description	Value
θ	angle of subduction	30°
g	gravitational acceleration	9.8 m^2 s^{-1}
x_0	characteristic length	100 km
u_0	characteristic velocity	10 mm yr^{-1}
ρ_0	characteristic density	3250 km m^{-3}
η_0	reference viscosity	10^{21} Pa s
T_0	reference temperature	1300°C
Q_0	reference activation energy	500 kJ mol^{-1}
n	power law exponent	3
R	gas constant	8.31 J mol^{-1} K^{-1}
t_0	characteristic time (x_0/u_0)	10^7 years
$\dot{\varepsilon}_0$	characteristic strain rate (u_0/x_0)	3x10^{-15} s^{-1}
τ_0	characteristic stress ($2\eta_0\dot{\varepsilon}_0$)	6 MPa
B	Byerlee's law gradient	60 MPa km^{-1}
Gr	Grashof number	100-1000

A strength profile of the lithosphere can be calculated from equation (2) provided that the strain rate, geotherm, and Byerlee's law constant are known. Figure 2b schematically illustrates the strength of a continental lithosphere that is subjected to a normal geotherm (Figure 2a). The strength of the upper crust and uppermost mantle is determined by Byerlee's law, whereas the strength of the lower crust and the lower part of the mantle lithosphere is determined by ductile flow. The vertically averaged strength of the lithosphere may decrease as a result of crustal thickening or temperature increase. Crustal thickening results in replacement of a strong uppermost mantle by a weak crust, which significantly decreases the total strength of the lithosphere (Figure 2c). A temperature increase (represented in Figure 2d as a perturbed geotherm, where the temperature field is 10-20% higher than a normal geotherm) affects the strength of both the crust and the mantle; however, the reduction in the strength of the uppermost mantle is more significant (Figure 2e). Horizontal compression is controlled by the strongest part of the lithosphere, which normally is the uppermost mantle. When the crust is thickened and/or the thermal profile is perturbed, the strongest region of the lithosphere can be the upper crust (e.g., Figure 2f).

Mathematical Formulation

We assume that the crust and the mantle behave as incompressible viscoplastic fluids. At stresses lower than the yield stress they are assumed to deform by power law creep (n = 3), and when the stresses have reached the yield stress, they deform plastically ($n \to \infty$). The equations that govern the power law creep are: force balance, continuity, and constitutive (stress-strain) relations. We do not attempt to

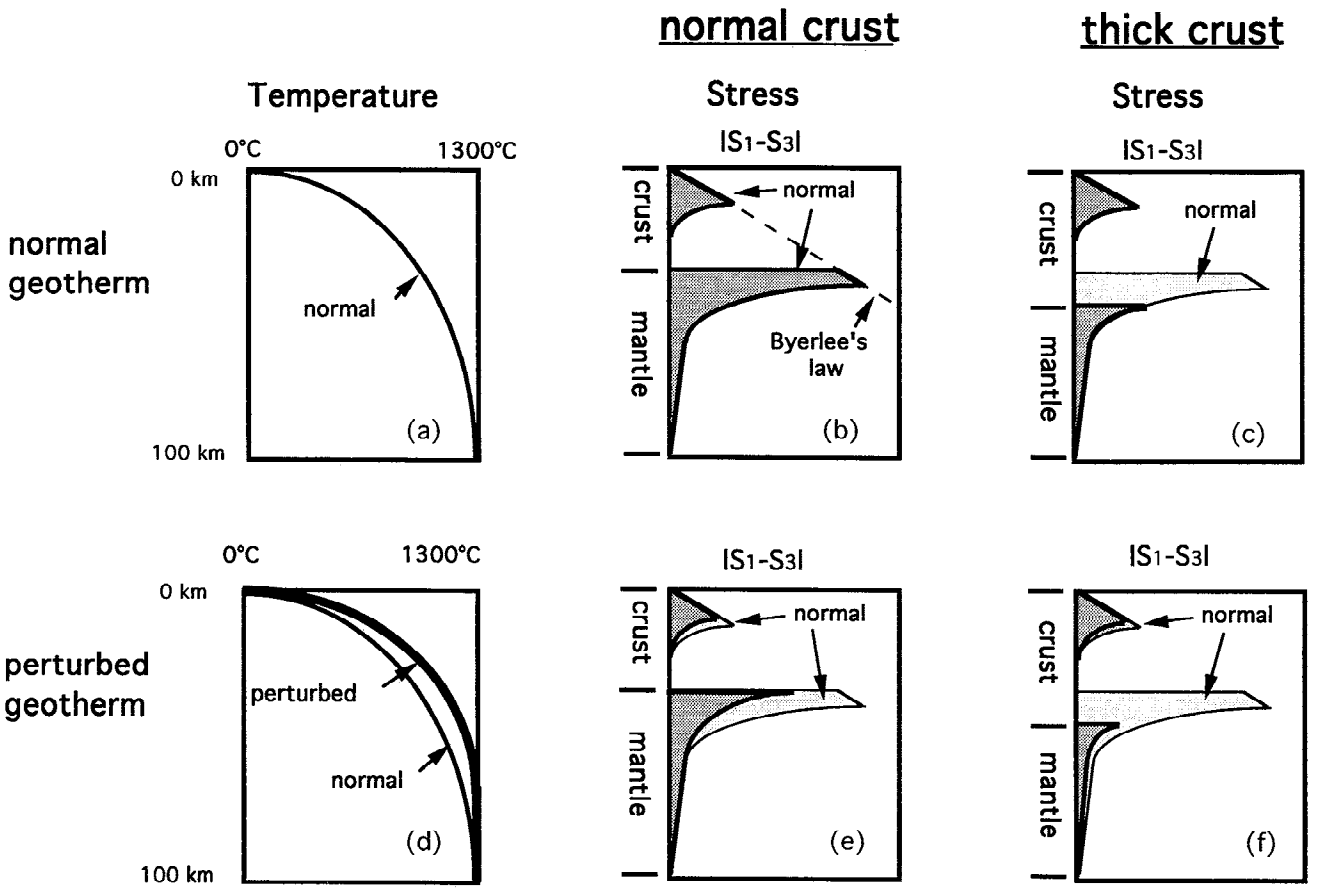

Figure 2. Schematic diagram showing (a) normal and (d) perturbed geotherms and their effect on the strength of the lithosphere (b) and (e) with normal crustal thickness and (c) and (f) with thickened crust. Both effects, thermal perturbation and crustal thickening, reduce the strength of the lithosphere. Higher temperature reduces the effective viscosity, whereas crustal thickening replaces the strong uppermost mantle with a very weak crust.

solve the energy equation because the thermal structure of the overriding plate depends on magmatism, formation of partial melts, and other complicated effects, the treatment of which is beyond of the scope of this paper. Instead, we impose a relatively simple thermal structure that enables us to calculate the effective viscosity.

The force balance equation with zero Reynolds number is

$$\sigma_{ij,j} = \rho\, g\, a_i \tag{4}$$

where σ_{ij} is the (i,j) component of the stress tensor, ρ is the density, g is the acceleration due to gravity, and **a** is the vertical unit vector (**a** = (0,0,1) in three dimensions and **a** = (0,1) in two dimensions). The continuity equation for incompressible fluids is

$$\nabla \cdot \mathbf{u} = 0 \tag{5}$$

where **u** is the velocity vector. The constitutive relations are

$$\tau_{ij} = 2\, \eta_{eff}\, \dot{\varepsilon}_{ij} \tag{6}$$

where τ_{ij} and are the (i,j) components of the deviatoric stress and strain rate tensors, respectively, and η_{eff} is the effective viscosity (see above). The deviatoric stress tensor is

$$\tau_{ij} = \sigma_{ij} + \delta_{ij}\, p \tag{7}$$

where δ_{ij} is Kronecker delta and p is the pressure ($p = -1/3\ \sigma_{kk}$). The strain rate tensor is

$$\dot{\varepsilon}_{ij} = \frac{1}{2}(u_{i,j} + u_{j,i}) \tag{8}$$

and its second invariant is

$$\dot{E} = \left(\dot{\varepsilon}_{ij}\, \dot{\varepsilon}_{ij}\right)^{1/2} \tag{9}$$

The second invariant of the strain rate tensor is used as the strain rate in the evaluation of the effective viscosity (3). By substituting (6), (7), and (8) into (4) and nondimensionalizing the equations, we obtain the following governing equations:

$$\begin{aligned} &\frac{\partial}{\partial x}\left[2\,\eta_{eff}\frac{\partial u}{\partial x}\right] + \frac{\partial}{\partial z}\left[\eta_{eff}\left(\frac{\partial u}{\partial z} + \frac{\partial v}{\partial x}\right)\right] - \frac{\partial p}{\partial x} = 0 \\ &\frac{\partial}{\partial x}\left[\eta_{eff}\left(\frac{\partial u}{\partial z} + \frac{\partial v}{\partial x}\right)\right] + \frac{\partial}{\partial z}\left[2\,\eta_{eff}\frac{\partial v}{\partial z}\right] - \frac{\partial p}{\partial z} = \rho\, Gr \end{aligned} \tag{10}$$

where u and v are the horizontal and vertical velocity components, respectively, and Gr is the nondimensional Grashof number

$$Gr = \frac{g \rho_0 x_0^2}{\eta_0 u_0} \quad (11)$$

The parameters x_0, u_0, η_0, and ρ_0 are the characteristic, length, velocity, viscosity, and density, respectively (Table 1). The Grashof number represents the ratio between buoyant and viscous forces [*Turner*, 1973; *Wdowinski and O'Connell*, 1991]. Because we choose a lower characteristic viscosity and velocity than the values used by *Wdowinski and O'Connell* [1991], the value of the Grashof number is larger here by an order of 10^2-10^3. We define another nondimensional parameter, the slip layer stress

$$\tau_s = \frac{\eta_s u_s / x_s}{\eta_0 u_0 / x_0} \quad (12)$$

where x_s, u_s, and η_s, are the slip layer length, velocity, and viscosity, respectively. This parameter represents the shear stress that the subducting plate exerts on the overriding plate along the slip layer.

Thermal Structure and Choice of Parameters

We ignore the complex thermal structure of the overriding plate by assuming simple thermal structure. The surface temperature of the lithosphere is assumed to be 0°C and the basal temperature is assumed to be 1300°C [e.g., *Turcotte and Schubert*, 1982, p. 7]. The temperature gradient within the lithosphere is assumed to be high near the surface and to decrease with depth, which reflects lithospheric heat transfer by conduction and heat generation within the crust. We describe this geotherm by a simple mathematical expression

$$T(z) = T_0 (1 + \varepsilon_T) \sqrt{\frac{z_s - z}{z_s - z_b}} \le T_0 \quad (13)$$

where T(z) is the temperature at depth z, T_0 is the temperature at the base of the lithosphere (1300°C), ε_T is thermal perturbation, and z_s and z_b are the vertical location of the surface and the base of the lithosphere, respectively. The thermal perturbation is a quantity ($-1 \le \varepsilon_T \le 1$) that describes the deviation of the vertical thermal profile from the normal square-root profile. Because we assume that the maximal lithospheric temperature is T_0, any calculated temperature (T(z)) that exceeds this value is set to T_0. In some of the calculations we assume a horizontal uniform geotherm (ε_T = 0), whereas in others we impose a higher geotherm (ε_T = 0.02-0.2) above the wedge tip, which represents a possible thermal effect beneath the volcanic arc. We also consider a negative thermal perturbation (ε_T = -0.2) caused by heat conduction from the hot lithosphere to the cold slab and impose it in a narrow zone (50 km wide) adjacent to the subducting slab. This effect downwarps the isotherm by 200-400°C [e.g., *Turcotte and Schubert*, 1982, p. 196].

Our formulation requires a priori determination of three material properties: density (ρ), activation energy (Q), and preexponent (A) (Table 2). We consider the density structure of buoyant granitic crust (ρ_c = 2700 kg m^{-3}) overlying a denser peridotitic mantle (ρ_m = 3250 kg m^{-3}). Density variations due to thermal expansion are ignored, because they are less than 2%, and lie within the error of the density estimation. We use experimental data of olivine creep to estimate the mantle activation energy (Q_m), and quartz creep data to obtain the crustal activation energy (Q_c). The olivine and quartz activation energies depend on grain size, water content, and oxidation state. The olivine activation energy lies in the range 450-600 kJ mol^{-1} and that of quartz in the range 150-200 kJ mol^{-1} [*Goetze*, 1978; *Brace and Kohlstedt*, 1980; *Kirby and Kronenberg*, 1987]. The experimental value of quartz activation energy results in an unrealistically weak crust. We therefore follow *Christensen* [1992] and raise the range of crustal activation energy to 150-320 kJ mol^{-1}. A_m is implicitly specified by the choice of the other characteristic parameter (η_0, T_0, Q_0, etc.). However, we need to specify the ratio of the crustal to the mantle preexponents, which is assumed, for simplicity, to be 1 (A_c = A_m). The slip layer, which is weaker than both the crust and the mantle, is assumed to behave as a Newtonian fluid (n = 1) with a low preexponent value (A_s = 0.01-0.1 x A_m).

Boundary and Initial Conditions

Along the upper surface of the model, which is Earth's surface, we impose a traction free boundary condition. This condition allows the upper surface to deform and to develop topography. Along the lower surface, which is the lithosphere-asthenosphere boundary, we also impose a traction free condition but impose lithostatic pressure, because the asthenosphere is assumed to behave as inviscid fluid. We have chosen to neglect basal tractions because their contribution in a temperature dependent viscoplastic rheology is negligible. This is in contrast to previous studies of deformation above subduction zones [*Wdowinski et al.*, 1989; *Wdowinski and O'Connell*, 1991], where Newtonian rheology that produces significant basal tractions is assumed. We choose to keep the horizontal location of the trench stationary and to impose the horizontal component of the convergence velocity (u_h) along the vertical right side boundary. The subduction component of the convergence velocity (u_s) is imposed along the slip layer.

Dunber and Sawyer [1989] suggested that preexisting weaknesses control the style of continental breakup. Following their suggestion, we also investigate the effect of preexisting weaknesses on large-scale compressional deformation. The starting model normally assumes a laterally uniform lithospheric geometry, where the continental crust is everywhere 35 km thick. However, some starting models consider the effect of an initially thick crust confined to a finite region above the asthenospheric wedge tip because crustal thickening tends to weaken the strength of the lithosphere (Figure 2). The initially thick crust simulates a possible scenario of an active plate margin (e.g., northern Andes) that likely precede a mountain building phase.

Method of Solution

The governing equations (10) are solved numerically via a finite element technique that uses eight-noded isoparametric elements and a penalty function formulation. The penalty function replaces the pressure term for an incompressible fluid and is solved by a selective reduced integration technique [*Zienkiewicz and Taylor*, 1991, p. 518-534]. The velocity field is solved at successive time steps because the governing equations are time independent. At each time step we calculate the geometry of the finite element mesh (see below), impose

the depth dependent temperature structure, and solve for the velocity field. We use an iterative technique to solve the governing equations, because the effective viscosity is velocity dependent. At each iteration the effective viscosity is calculated according to the previously calculated velocity and used to determine the new velocity field. We iterate until the largest velocity difference between two iterations is sufficiently small ($|u_i-u_{i-1}|/|u_i| < 0.001$). For the first iteration of the first time step, we need to use a Newtonian rheology (velocity independent) to obtain the first calculated velocity field. As a result, the solution of the first time step requires about 25 iterations, whereas other time step solutions are obtained with typically 5-10 iterations. Various numerical experiments with 200-800 elements and 100-3000 time steps have been conducted to ensure that the solutions are grid and time stepping independent.

Throughout the calculations, the boundary conditions, which represent the tectonic forces, remain constant, but the surfaces on which the conditions are applied evolve with time. Thus the evolution of the deformation is determined by the buoyancy forces, which vary as the topography and crustal thickness evolve. At the initial time step, the topography and the Moho are set according to the initial model configuration. At later stages, the topography and Moho configurations are updated in a Lagrangian manner by assuming constant velocity between two successive time steps. Because we assume removal of the lithospheric mantle, the configuration of the lithosphere-asthenosphere boundary does not change as the calculations proceed. At each time step the finite element mesh is deformed according to the velocity field of the previous time step. In order to avoid excessive deformation of some elements in the localized zone of deformation, the mesh is reorganized according to the new location of the upper surface and Moho. Similarly, the position of the mesh points in the slip layer are updated in a manner that keeps the slip layer parallel to the subducting slab.

Results

One of the main characteristics of power law rheology is localization of the deformation at regions of high stress or strain rate level. Such a localization, which is characteristic of deformation of continental lithosphere, develops if the initial stress field is perturbed but does not occur if the initial stress field is uniform. The two main mechanisms that weaken continental lithosphere and lead to localization of lithospheric deformation are thermal perturbation and crustal thickening (Figure 2). In this section we present results of various calculations of lithospheric deformation that consider these two mechanisms and produce a finite region of localized deformation and high elevated plateaus.

By using a finite element technique, we obtain numerical solutions for the velocity, viscosity, and strain rate fields within the lithosphere at each time step. The configuration of the finite element mesh indicates the surface topography and crustal structure as the lithosphere deforms. We chose to demonstrate our results by using an example of a deformed lithosphere that has been subjected to 300 km of horizontal shortening during 3 time units (30 m.y.) (Plate 1). In this example we assume an initially uniform crustal thickness of 35 km and impose a thermal perturbation in a 600-km-wide region from the wedge tip inland, in which the geotherm is 10% higher than a normal geotherm ($\varepsilon_T = 0.1$). The model produces surface topography that can be divided into three regions: below sea level near-trench topography, high topography above the thickened crust, and close to sea level topography farther inland. The imposed temperature field of the lithosphere (Plate 1a) reflects a normal geotherm far from the trench and a perturbed geotherm near the trench. Along the contact with the subducting slab the isotherms are deflected downward due to conduction of heat from the hot lithosphere to the cold downgoing slab and due to the low topography at the trench. Between the wedge tip and 600 km inland, the isotherms are deflected upward due to the imposed perturbed geotherm and the high topography.

The temperature field (Plate 1a) is imposed for each time step and is used to evaluate the effective viscosity (Plate 1b), velocity, and strain rate fields (Plates 1c and 1d). The high-viscosity regions (Plate 1b) are the upper crust, the uppermost mantle, and the region along the subducting slab. The high-viscosity reflects material properties combined with relatively low temperatures. The low-viscosity regions are the slip layer, which is assumed to behave as a weak Newtonian fluid, and the lower crust. The region near the wedge tip has a low viscosity because of the high temperature and the high degree of deformation that are localized in this region. The normal strain rate field (Plate 1c) shows a localization of compressional deformation ($e_{zz} = -e11$) near the wedge tip in the mantle part of the lithosphere. The compressional deformation in the crust is more diffuse and tends to concentrate within a few hundred kilometers inland from the wedge tip on the topographic slopes, because the thick crust and high topography induce buoyancy forces that resist the indentation. The shear strain rate (Plate 1d) is concentrated in the weak lower crust, which acts as a shear zone that decouples the upper crust from the mantle.

The evolution of the topography, crustal thickness, velocity and strain rate fields of three types of calculations are shown in Plates 2 and 3 and Figure 3. These calculations differ form one another in their initial crustal structure and in their thermal structure. Solutions for laterally uniform lithosphere (Figure 3c) indicate that the deformation, crustal thickness, and topography are uniformly distributed along the entire length of the lithosphere. Although power law rheology is used, no localization of the deformation occurs because the strain rate field is uniform. However, when a horizontal thermal perturbation or an initially thick crust, are introduced, the deformation, crustal thickening, and topography are localized in the weak region near the wedge tip (Plates 2 and 3 and Figures 3a and 3b). In the three models, the near-trench topography, which is dynamically supported, approaches a steady state configuration within the first two time units. However, the topography above sea level rises steadily as the crust thickens, and the size of the plateau increases with time. The mountain topography, which is mostly isostatically compensated, reflects the Moho topography.

Although calculations for thermally perturbed lithosphere and initially thick crust both localize the deformation near the wedge tip, the shape of their calculated topography differ significantly (Figures 3a and 3b). The thermally perturbed lithosphere produces a high elevated plateau with a wavelength of the thermal perturbation, whereas the initially thick crust develops a monocline with a steep slope toward the trench and a gradual slope inland. The two calculations use two wavelengths of perturbations (600 km for the case of higher geotherm versus 250 km for the case of initially thick crust),

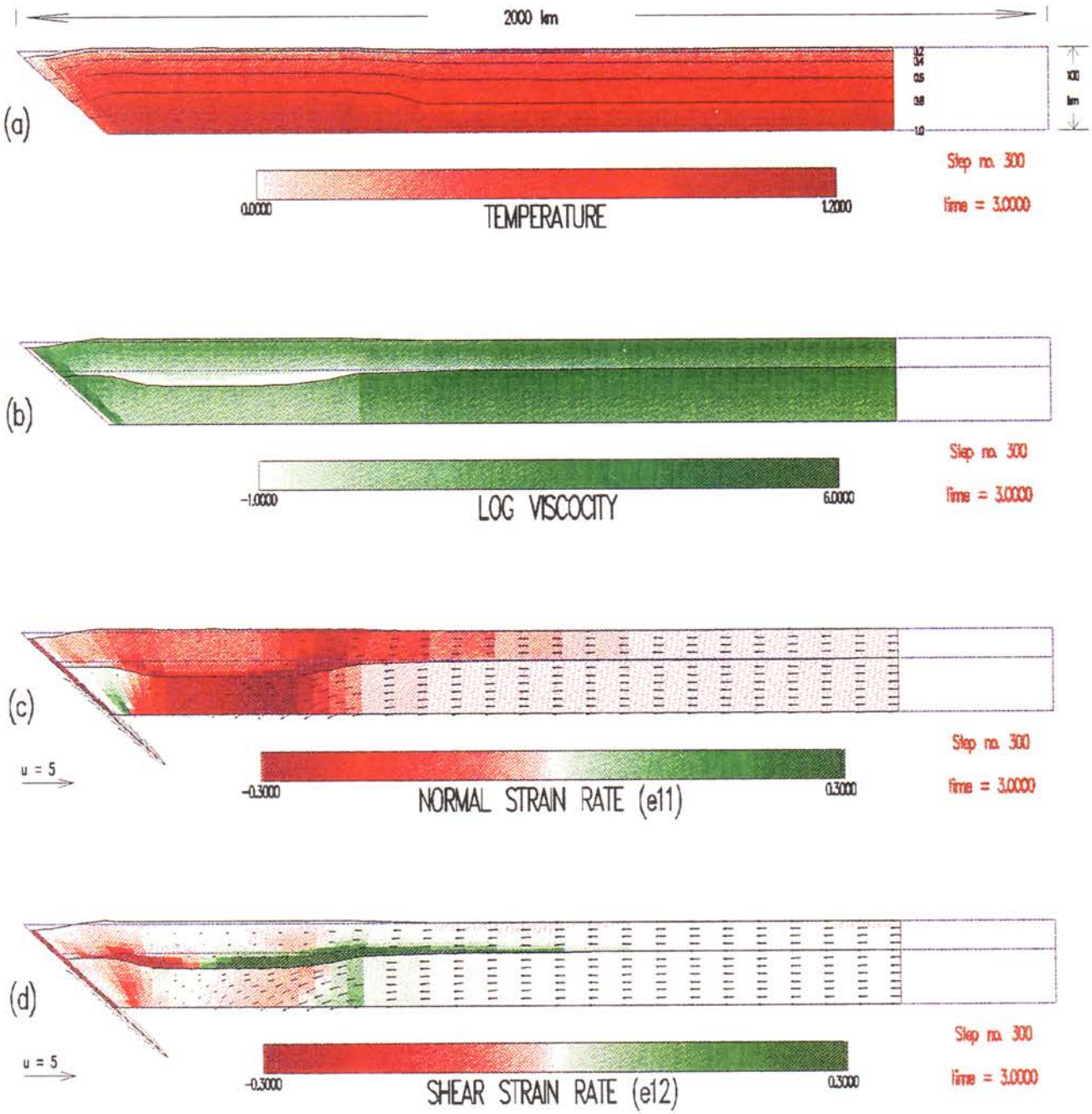

Plate 1. (a) Temperature, (b) effective viscosity, (c) normal strain rate and velocity, and (d) shear strain rate and velocity fields of thermally perturbed lithosphere that has been subjected to 300 km of shortening during three time units (30 m.y.). The thermally perturbed region extends from the wedge tip 600 km inland and its geotherm is 10% higher ($\varepsilon_T = 0.1$) than the normal square-root geotherm. The blue lines indicate the initial lithospheric configuration.

because we try to compare two possible scenarios that may lead to the development of a 600-km-wide plateau. The width of the initially thick crust is obtained from various mountain belts that override subduction zones (e.g., the northern or southern segments of the Andes), whereas the width of the thermal perturbation is arbitrarily imposed. The sensitivity of the results to the wavelength of the thermal perturbation is presented in the following section (in particular in Figure 4a).

The evolution of the deformation in Plates 2 and 3 shows an inland migration with time of the locus of the crustal deformation. As the crust thickens, it induces buoyancy forces that tend to relax the horizontal density contrast by distributing the buoyant crust over a larger region, rather than by thickening the crust in one location. However, the locus of the deformation of the mantle lithosphere remains near the wedge tip throughout the calculations at the weakest part of the mantle lithosphere. The two deformation patterns differ from one another by the wavelength of the localized deformation and its horizontal location. In the thermally perturbed lithosphere (Plate 2), most of the mantle

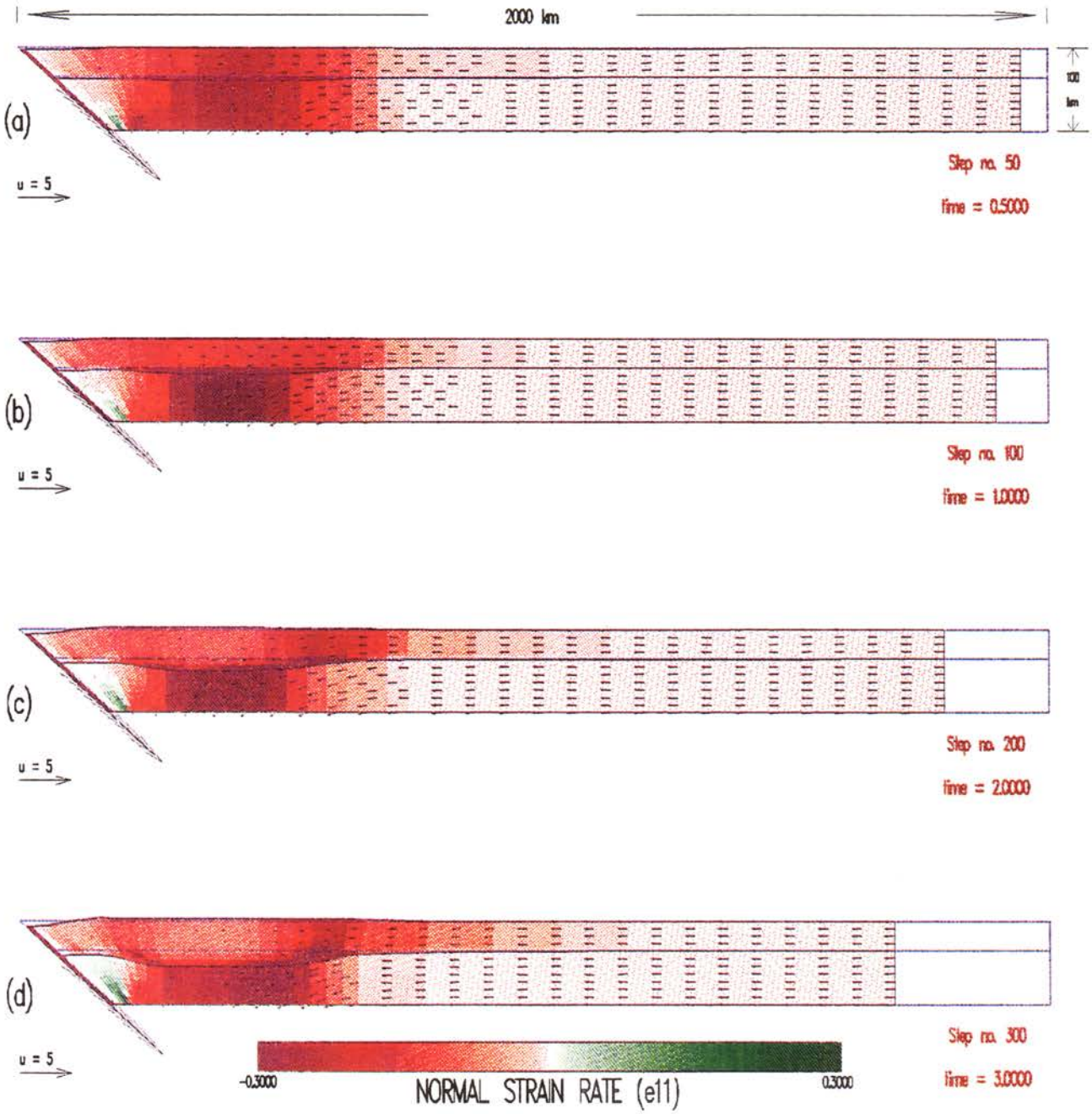

Plate 2. Calculated topography, crustal structure, and normal strain rate (e11) at four time steps during the deformation of a thermally perturbed lithosphere. The thermally perturbed ($\varepsilon_T = 0.1$) region extends from the wedge tip 600 km inland. The compressional deformation (red) of the mantle lithosphere is localized at the thermally perturbed weak region near the wedge tip at all time steps. However, the crustal compressional deformation diffuses with time and migrates inland.

compressional deformation occurs within the thermally perturbed region with further localization beneath the thickest region of the crust, whereas in the initially thick crust (Plate 3) the mantle deformation localizes in a narrower region, beneath the thickest crust. The crustal compressional deformation is more localized in the thermally perturbed lithosphere and most of the deformation occurs within the perturbed region, whereas in the initially thick crust the locus of the deformation diffuses with time and migrates farther inland.

Sensitivity Studies

So far, we have presented results of three types of calculations: laterally uniform lithosphere, thermally perturbed lithosphere, and initially thick crust. High topography is produced by models that include a thermally perturbed lithosphere or an initially thick crust; however, only the thermally perturbed lithosphere solutions produce a high elevated plateau of realistic shape. These solutions depend on several parameters, each of which can affect the

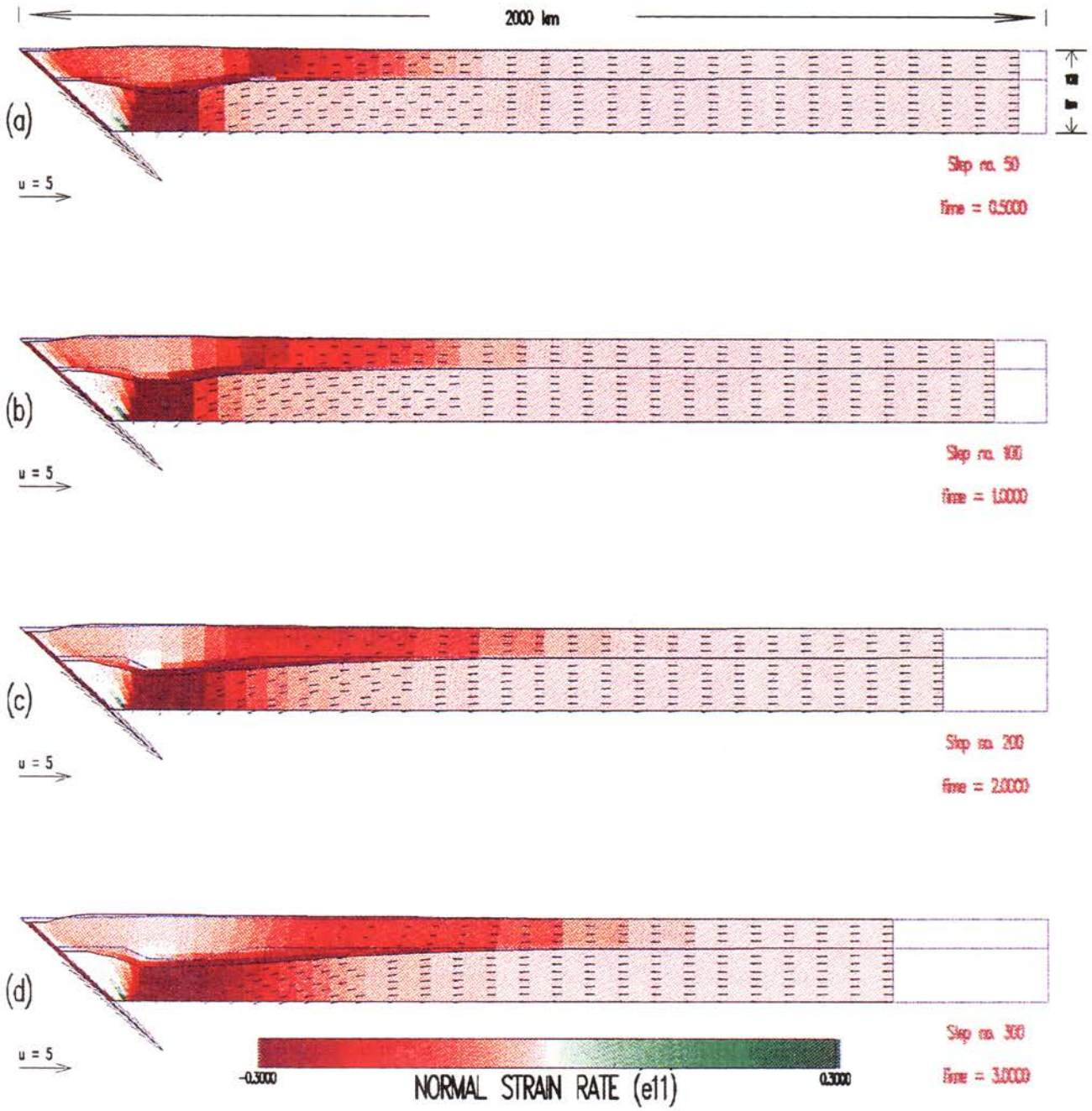

Plate 3. Calculated topography, crustal structure, and normal strain rate (e11) at four time steps during the deformation of a lithosphere with initially thick crust; the 50-km-thick crust extends from the wedge tip 100 km inland, and the transition between normal thickness (35 km) to the thick crust occurs over 100 km over both sides of the thick crust. The compressional deformation of the mantle lithosphere is localized near the wedge tip at all time steps. However, the crustal compressional deformation diffuses with time and migrates inland.

calculated deformation and topography. In this section we present results of various calculations that demonstrate the sensitivity of the solution to the various parameters, which illustrate the physics behind the model. The sensitivity studies present results for a thermally perturbed lithosphere, but some of these are also applicable to the two other types of models. Although our model solves for the topography, crustal thickness, viscosity, strain rate, and velocity fields, we present mostly the calculated topography, which is most easily tested against observations.

First, we investigate the sensitivity of the model to the assumed thermal structure (Figure 4). We impose a uniform geotherm along the lithosphere, except along the slip zone where the isotherms are deflected downward, and near the wedge tip where they are deflected upward. Because we are mostly concerned with the evolution of elevated plateaus and less with the trench topography, we only investigate the upward deflection of the isotherms near the wedge tip. We do this by varying the wavelength and the amplitude of the thermal perturbation. Figure 4a shows that the width of the

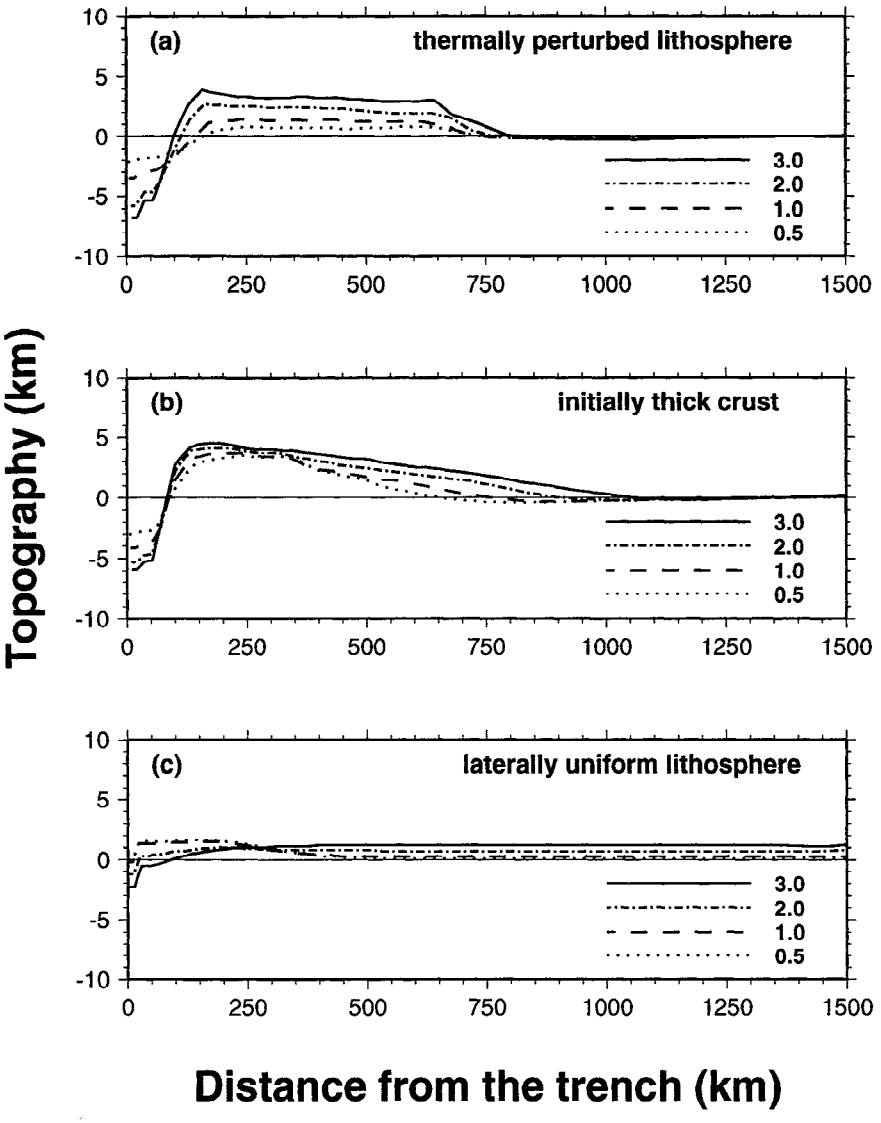

Figure 3. Calculated topography at four time steps during the deformation of three types of calculations. (a) The topography of the thermally perturbed lithosphere (as in Plate 2) is localized near the wedge tip and has the shape of a high elevated plateau with a wavelength of the thermal perturbation. (b) The topography of the initially thick crust (as in Plate 3) is also localized near the wedge tip, but it forms a monocline with a steep slope toward the trench and a gradual slope inland. (c) The topography of the laterally uniform lithosphere is distributed uniformly along the entire length of the lithosphere. In the three cases, the near-trench topography, which is dynamically supported, approaches a steady state configuration within the first two time units. However, the above sea level topography rises steadily as the crust thickens, and the size of the plateau increases with time.

plateau is controlled by the wavelength of the thermal perturbation. Because of buoyancy forces, continental crust cannot be thickened beyond 60-70 km, which dictates a maximum plateau elevation of 4-6 km. When the width and the height of the plateau and the thickened crust beneath are too small to accommodate all the volume of the shortened crust, the excess volume is added adjacent to the plateau, generating a gradual slope inland (dotted line in Figure 4a). When the width of the thermally perturbed region is wide enough to accommodate all of the shortened crustal material, the shape of the plateau reflects the wavelength of the perturbation. Figure 4b shows that the solutions are not very sensitive to the amplitude of the perturbation, although minor variation can be detected. Figure 4c shows that for short to medium width plateaus, the plateau shape reflects the maximum wavelength of the perturbation when the wavelength increases with time. However, perturbations with long wavelength that increase with time tend to generate a monocline.

The evolution of the plateau topography strongly depends on the assumed thermal structure. When the wavelength of the thermal perturbation is wide and constant with time, the plateau width is uniform, but its height increases with time; the plateau rises upward steadily at a nearly uniform rate (Figure 5a). However, when the wavelength of the perturbation increases with time, the elevation of the plateau is uniform, but the plateau width increases with time (Figure 5c). A

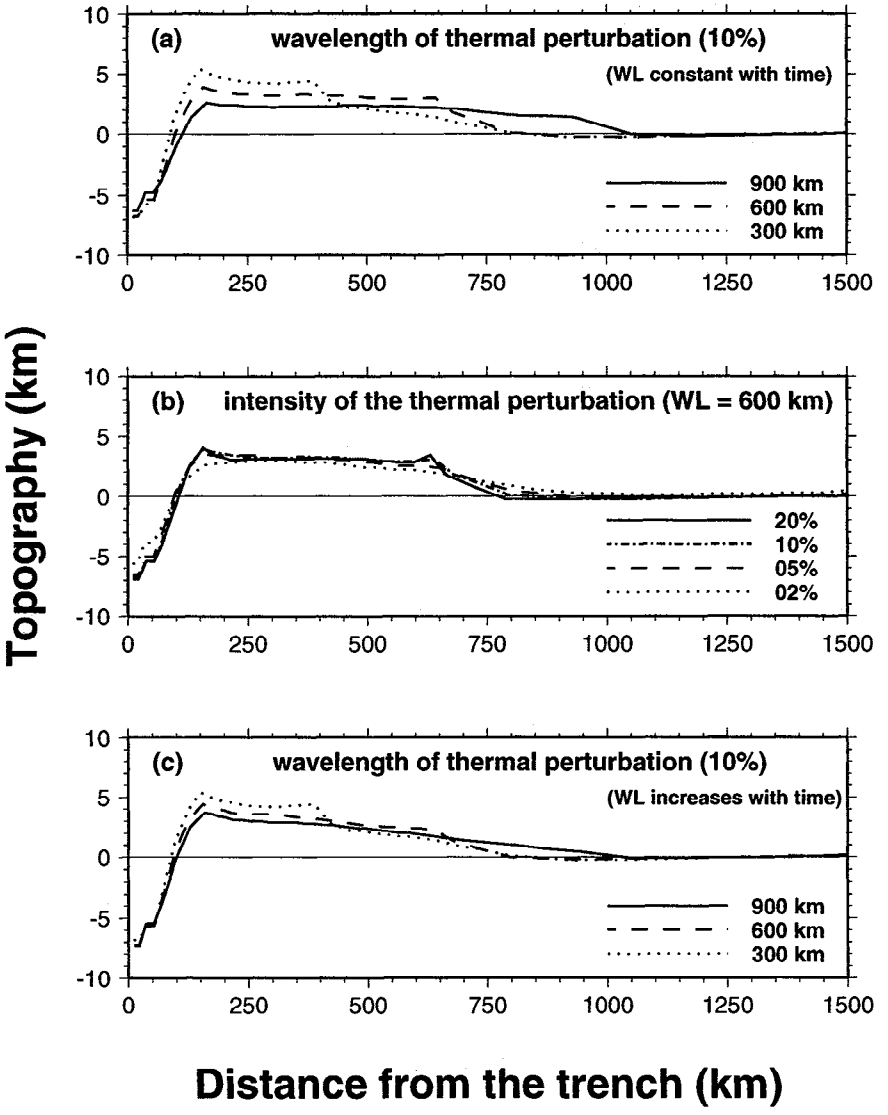

Figure 4. Sensitivity of the calculated topography of a lithosphere that has been subjected to 300 km of shortening during three time units to (a) the wavelength of the perturbation (ε_T = 0.1) that is kept constant with time, (b) the amplitude of a 600 km wide perturbation, and (c) the wavelength of the perturbation (ε_T = 0.1) that is initially 100 km wide and increases with time.

different evolution pattern was suggested by *England and Houseman* [1989], who proposed that the plateau uplift occurs in two stages: crustal thickening gradually followed by lithospheric thining and uplift of the plateau. In order to resolve an accurate uplift history, we need to consider a more detailed thermal structure, which is beyond the scope of this paper.

The model produces two types of topography: near-trench dynamically supported topography, and inland isostatically supported topography. The magnitude of both types of topography depends on the Grashof number (Gr), which represents the ratio of buoyancy to viscous forces. Figure 6a shows that the magnitude of the topography decreases with Gr. A physical explanation for the dependency of the topography and Gr can be derived from the balance between tectonic and buoyancy forces. As Gr increases, the effect of buoyancy forces increases with respect to the tectonic forces. At a high value of Gr, the balance between the two forces can be reached only if the magnitude of the topography decreases, as shown in Figure 6a. The magnitude of near-trench dynamically supported topography also depends on the slip layer stress (τ_s), which determines the force that the subducting slab exerts on the overriding plate (equation (12)). Figure 6b shows that near trench topography increases with the slip layer stress. Again, in order to keep the balance between tectonic and buoyancy forces, the increased tectonic forces are balanced by higher-magnitude buoyancy forces induced by higher-magnitude near-trench topography. Details of the modeling and results of the near trench topography are presented by *Wdowinski* [1992]. The magnitude of the inland isostatically supported topography depends on Gr and on the ratio of crustal to mantle density (ρ_c/ρ_m). Figure 6c shows that the magnitude of the topography decreases as the density ratio increases, which is simply an outcome of isostasy.

The rheological parameters also significantly affect the deformation and topography patterns. We present a few results

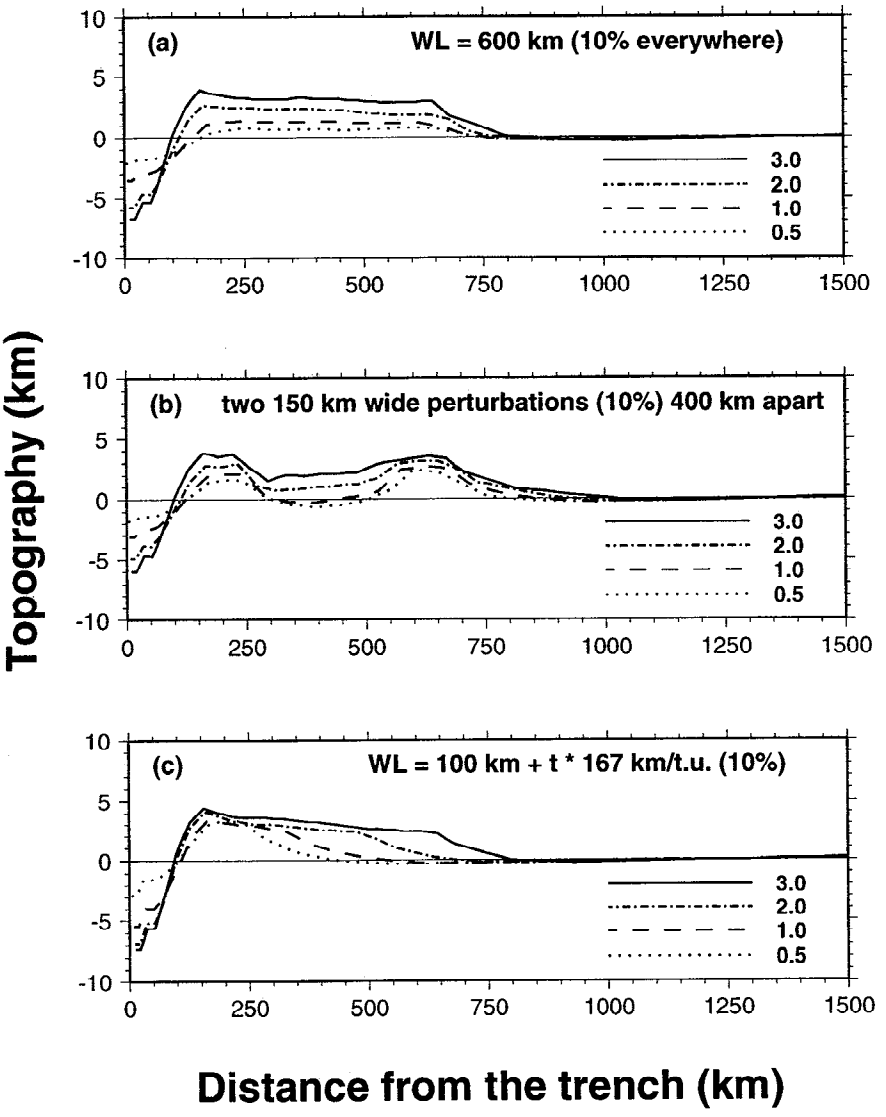

Figure 5. Calculated topography at four time steps during the deformation of three cases that differ from one another by their thermal structure. (a) The thermal perturbation (ε_T = 0.1) is 600 km wide, evenly distributed, and kept constant throughout the calculations. (b) Two 150-km-wide perturbations (ε_T = 0.1) are located 400 km apart. (c) The thermal perturbation (ε_T = 0.1) is initially 100 km wide, and its width increases with time.

that demonstrate qualitatively the sensitivity of the model to changes in strength of the crust and mantle. The reference model, which uses the default material property values (Table 2), is shown in Plates 4a and 4b. We chose to vary the crustal and mantle activation energies (Q_c and Q_m), although similar results can be obtained by varying the preexponent values (A_c and A_m), the Byerlee's law constant (B), or the thermal structure (T(z) in equation (13)). An increase in the mantle activation energy (Q_m) increases the effective mantle viscosity (Plate 4c), which tends to further localize the zone of mantle compressional deformation (Plate 4d). However, the pattern of the crustal deformation, crustal structure, and topography are not very sensitive to the change in the strength of the mantle. Changes in the crustal activation energy (Q_c) hardly affect the mantle viscosity and deformation but produce significant changes in the effective crustal viscosity, deformation pattern, and topography. A decrease in crustal activation energy increases the thickness of the weak lower crust and decreases the thickness of the strong upper crust (Plate 4e), which results in a very diffuse crustal compressional deformation pattern (Plate 4f). An increase in the crustal activation energy reduces the thickness of the weak lower crust, or completely eliminates it as shown in Plate 4g. The result is localization of the crustal and mantle deformation in the weak region that is thermally perturbed. Changes in the near trench topography are an outcome of a force balance change as the strength of the crust varies without changing the forces that deform it. The reference model (Plates 4a and 4b) produces a 5-km-deep dynamically supported topography, whereas the solution for the case of a weaker crust produces a deeper trench and the solution for the case of a crust as strong as the mantle does not produce a trench topography at all.

Discussion

Formation of high elevated plateaus was also studied by thin viscous sheet (TVS) models [e.g., *England and McKenzie*, 1982]. Our temperature dependent viscoplastic models (TDVP)

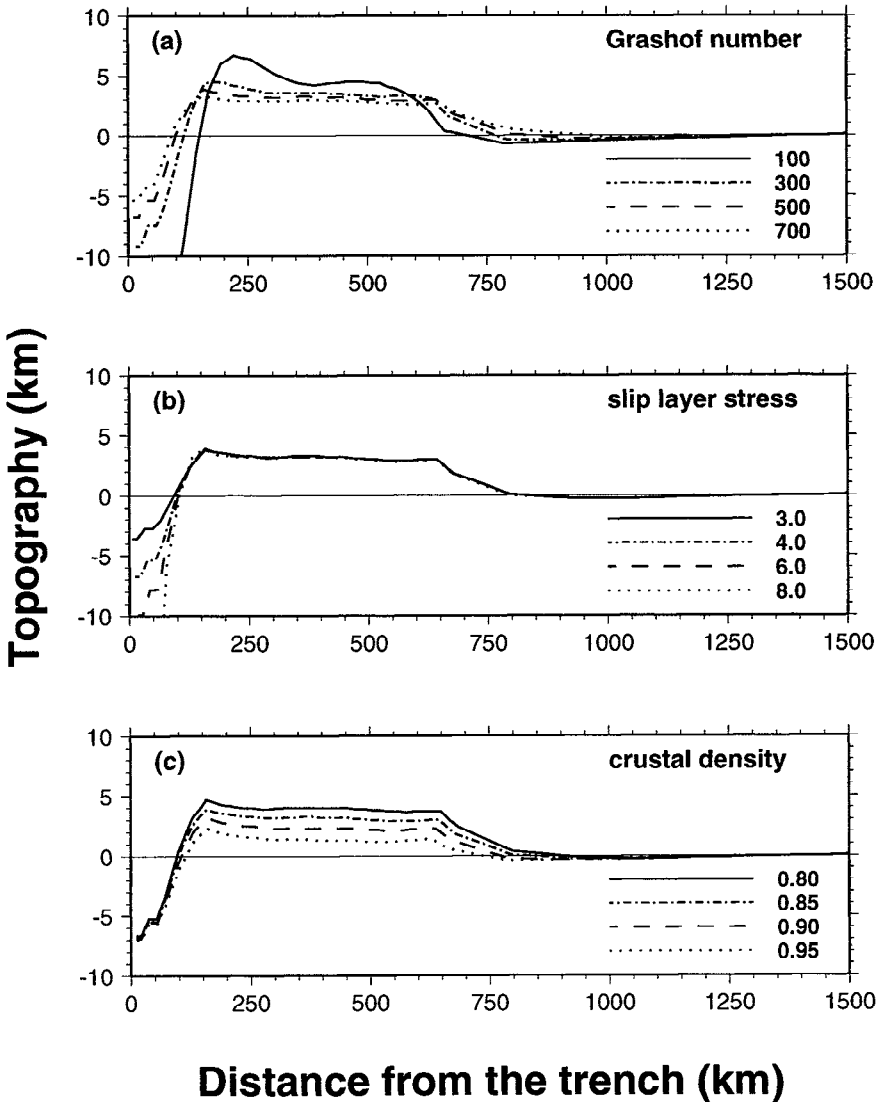

Figure 6. Sensitivity of the calculated topography of a thermally perturbed lithosphere (ε_T = 0.1) that has been subjected to 300 km of shortening during three time units to (a) the Grashof number, (b) slip layer stress, and (c) crustal density.

Table 2. Nondimensional Values of Material Properties Used in the Calculations

Property	Value		
	Crust	Mantle	Slip Layer
Power law exponent n	3	3	1
Activation energy Q	0.5-1.0 (0.65)	1.0-1.1 (1.0)	-
Preexponent A	1.0 (1.0)	1.0 (1.0)	0.05-0.15 (0.075)
Density ρ	0.8-0.95 (0.85)	1.0 (1.0)	0.8-0.95 (0.85)

Default values are shown in parentheses.

differ from the TVS models in the basic assumptions: (1) The TVS use a two-dimensional horizontal map view approximation, whereas the TDVP models use two-dimensional vertical plane strain approximation. (2) The TVS models assume depth independent rheology and deformation, whereas the TDVP models assume depth dependent rheology and deformation. (3) The TVS models assume only horizontal indentation of the boundary and use sinusoidal-shaped boundary conditions, whereas the TDVP models take into account both horizontal and vertical forces at the indenting boundary, but the indentation is uniform with depth. (4) The TVS models usually assume homogeneous strength of the lithosphere, whereas the TDVP models take into account strength variations due to thermal effects.

TVS models, although successfully predicted the long-wavelength topography of the plateau, failed to produce the flat plateau topography [e.g., *England and McKenzie*, 1982]. These model generally produce a monocline-shaped topography similar to the results of our initially thick crust

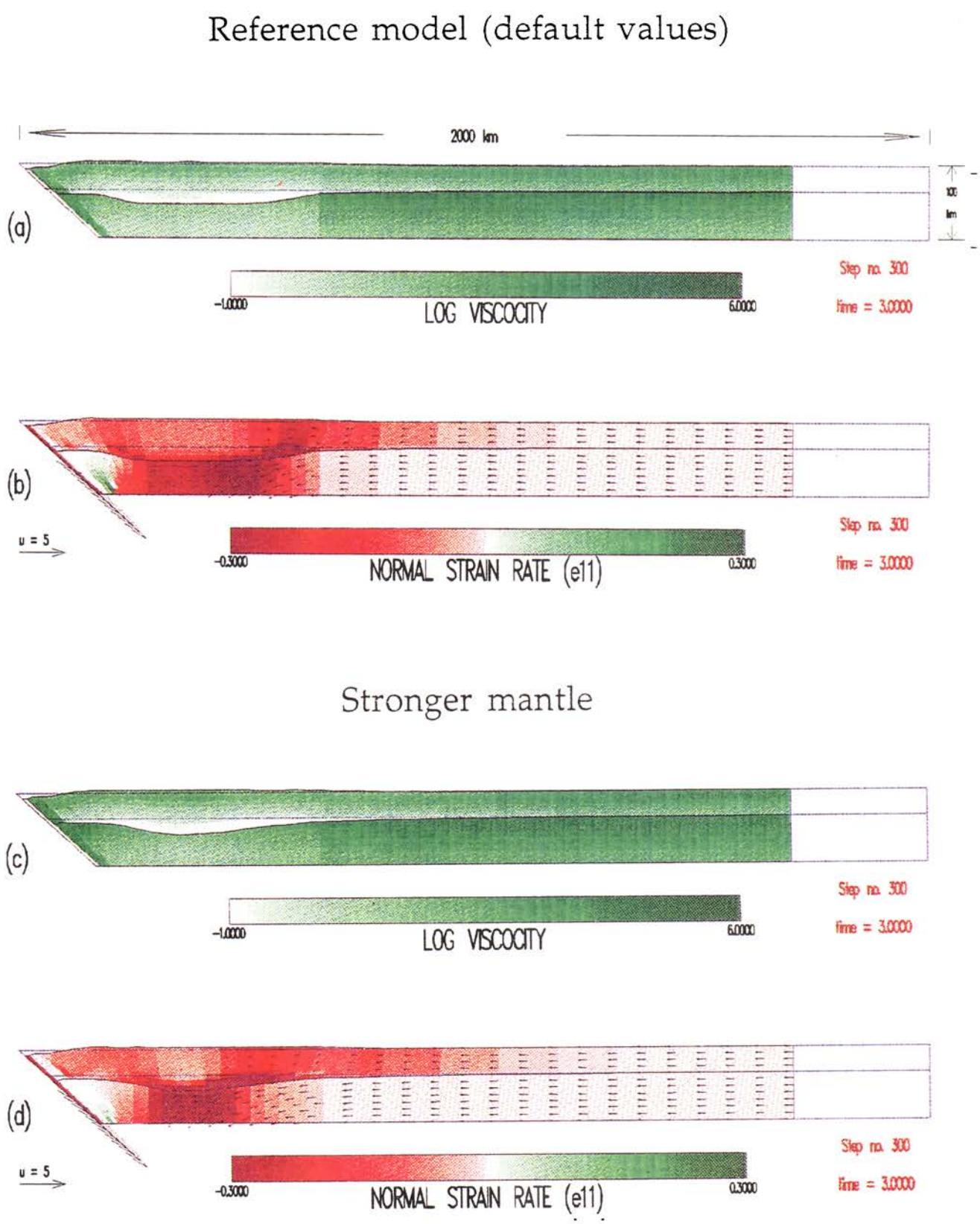

Plate 4. Sensitivity of the solutions to the activation energy of the crust and mantle. (a) and (b) Calculated effective viscosity, topography, crustal structure, strain rate, and velocity fields with the default values (Q_c = 325 ; Q_m = 500 kJ mol^{-1}). (c) and (d) Solution for stronger mantle (Q_c = 325 ; Q_m = 550 kJ mol^{-1}. (e) and (f) Solution for weaker crust (Q_c = 250 ; Q_m = 500 kJ mol^{-1}). (g) and (h) Solution for stronger crust, as strong as the mantle (Q_c = 500 ; Q_m = 500 kJ mol^{-1}). The thermally perturbed lithosphere has been subjected to 250 km of shortening during 2.5 time units; the thermally perturbed (ε_T = 0.1) region extends from the wedge tip 600 km inland.

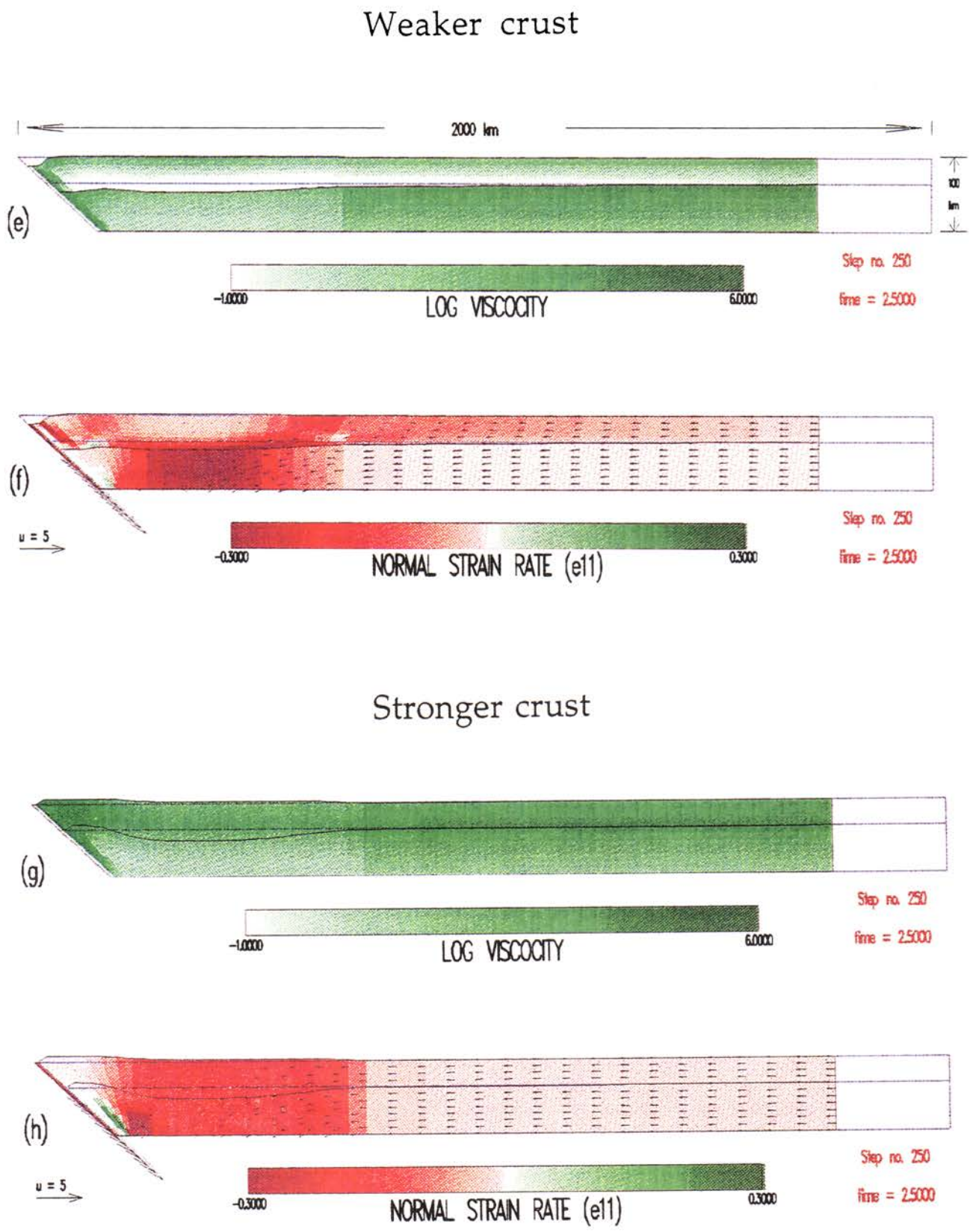

Plate 4. (continued)

model (Figure 3b). The only model that produces the plateau shape is the TDVP thermally perturbed model (Figure 3a) that assumes a localized zone of hot and weaker lithosphere of the same wavelength as the plateau. In addition, TVS models assume depth independent deformation and therefore cannot account for shear deformation in vertical planes. This shear deformation is characteristic to fold and thrust belts that often bound high elevated plateaus and is produced by the TDVP models.

Although a finite region of localized deformation and topography was produced by calculations for a thermally perturbed lithosphere or initially thick crust, only the first of these produces the topography of a high elevated plateau. This emphasizes the importance of considering temperature dependent rheology in studies of compressional continental deformation, as much as in studies of extensional deformation, where it is widely used [e.g., *Bassi*, 1991; *Christinasen*, 1992]. In this study we did not attempt to solve the temperature field because the thermal structure of the overriding plate involves magmatism, partial melts, and other complicated effects, which are beyond the scope of this paper. Instead, we imposed a relatively simple thermal structures that enabled us to calculate the effective viscosity and the deformation pattern. Because the deformation and topography patterns are strongly dependent on the thermal structure, future studies should attempt to include some of the thermal complexities and investigate their effects on the deformation.

The downward deflection of the isotherms along the subducting slab (Plate 1a) plays an important role in the calculations. Initially, we ignored this effect and assumed a normal geotherm along the contact with the subducting slab. As a result, the crust tended to thicken along the slip layer, because the shear deformation along the slip zone localized the deformation in that region. The near slip layer crustal thickening effect disappeared when we included the downward deflection of the isotherms in that region. This suggests that the overriding lithosphere is very strong along its contact with the subducting slab, as indicated by the high effective viscosity of that region (Plate 1b). The strength of the lithosphere along the subducting slab may explain the universal location of arc volcanism above the wedge tip and not closer to the trench [*Gill*, 1981]. This observation has generally been interpreted to reflect the melting curve of subducted rocks [e.g., *Gill*, 1981]. We suggest a mechanical explanation to this phenomenon, where a melt generated in the subducting slab cannot rise toward Earth's surface before it reaches the wedge tip, because it cannot penetrate the cold and strong overriding lithosphere between the trench and the wedge tip.

Wdowinski and O'Connell [1990] suggested that constant stress boundary conditions are more appropriate than constant velocity boundary conditions in continuum models of continental deformation. However, in this study we use constant velocity boundary conditions, because solutions with nonlinear rheology tend to be unstable when constant stress boundary condition were applied. The unstable solutions results from localization of stresses in narrow regions that produce high velocities as stresses are released. This behavior is unrealistic for the long timescale used in the model (10^5-10^7 years) but is very realistic at short timescales ($<10^3$ years), where the lithospheric deformation is dominated by earthquake ruptures. Although combining nonlinear rheology with stress boundary conditions is a difficult task, it should be addressed in the future, because it describes the more realistic and complex nature of lithospheric deformation.

Although the model successfully produces many aspects of the evolution of the topography and deformation of high elevated plateaus, it uses some assumptions that limit the applicability of the model. The two-dimensional flow assumption allowed us to avoid full three-dimensional computations, but as a result, we cannot obtain along-strike variations of topography and deformation, which plays an important role in the evolution of the Tibetan Plateau. We also assumed conservation of crustal material and therefore neglected various processes that may have affected the evolution of high elevated plateaus, such as weathering, tectonic erosion, accretion, and addition of mantle material to the crust (underplating). Finally, the imposed thermal structure of the lithosphere simplifies the contribution of important thermal processes, such as mantle delamination, magmatism, and partial melting; the details of these processes may be important in some areas.

Conclusions

The evolution of the deformation and topography of high elevated plateaus has been investigated using a temperature dependent viscoplastic flow model of the overriding continental plate. This rheology tends to localize the deformation in regions of anomalously weak lithosphere and simulates well the observed pattern of continental deformation. However, deformation localization occurs only when a strength perturbation is introduced to the lithosphere. When thermal or compositional weakening are introduced, the deformation, crustal thickening, and topography are localized in the weaker region. In both cases the topography rises from below sea level at the trench axis to a high elevated plateau at a height of a few kilometers above sea level and farther inland subsides gradually to about sea level. However, a high elevated plateau topography is produced only when the lithosphere is thermally weakened. The shape and size of the plateau depend on the wavelength of the thermal perturbation but are insensitive to the amplitude of the perturbation as long as the perturbation is higher than 5%. The plateau size (width and height) depends on the Grashof number and the density contrast between the crust and the mantle; both parameters determine the magnitude of the buoyancy forces relative to the tectonic forces.

The model shows that the evolution of high elevated plateaus is accompanied by a change in the deformation pattern. During the initial stages of the deformation, the loci of the crustal and mantle deformations coincide with one another, and the overall result is crustal thickening above the region of mantle delamination. As the deformation evolves and the crust thickens, it induces buoyancy forces of larger magnitude that tend to relax the thick crust and the mountain topography and therefore resist further accumulation of buoyant crustal material near the wedge tip. As a result, the locus of the crustal compressional deformation migrates inland and separates from the region where mantle compressional deformation is localized; the lower crust thus acts as a big shear zone. These results indicate that the deformation pattern in the upper crust does not always coincide with the deformation pattern in the uppermost mantle, especially during the later stages of deformation when the crust has been thickened. Furthermore, they show the

limitations of studies that assume depth independent deformation, such as in plane stress or thin sheet models.

Acknowledgments. We are grateful to Greg Houseman and the associate editor Martin Bott for very helpful comments. We would also like to thank Ximena Barrientos, Mark Everett, and Scott King for helpful discussions and comments. This work was supported by NSF grants EAR-8817067 and EAR-9004367. Part of the first author's salary was provided by the Ida and Cecil Green Fellowship.

References

Ashby, M. F., and R. A. Verrall, Micromechanisms of flow and fracture, and their relevance to the rheology of the upper mantle, *Philos. Trans. R. Soc. London*, ser. A, 288, 59-95, 1977.

Bassi, G., Factors controlling the style of continental rifting: Insights from numerical modeling, *Earth Planet. Sci. Lett.*, 105, 430-452, 1991.

Bird, P., Laramide crustal thickening event in the Rocky Mountain foreland and Great Plains, *Tectonics*, 3, 741-758, 1984.

Bird, P., Formation of the Rocky Mountains, western United States: A continuum computer model, *Science*, 239, 1501-1507, 1988.

Bird, P., New finite element techniques for modeling deformation histories of continents with stratified temperature-dependent rheology, *J. Geophys. Res.*, 94, 3967-3990, 1989.

Brace, W. F., and D. L. Kohlstedt, Limits on lithospheric stress imposed by laboratory experiments, *J. Geophys. Res.*, 85, 6248-6252, 1980.

Burchfiel, B. C., and G. A. Davis, Nature and controls of Cordilleran orogenesis, western United States: Extensions of an earlier synthesis, *Am. J. Sci.*, 275-A, 363-394, 1975.

Byerlee, J. D., Friction of rocks, *Pure Appl. Geophys.*, 116, 615-626, 1978.

Chery, J., J. P. Vilotte, and M. Daignieres, Thermomechanical evolution of a thinned continental lithosphere under compression: Implications for the Pyrenees, *J. Geophys. Res.*, 96, 4385-4412, 1991.

Christensen, U. R., An Eulerian technique for thermomechanical modeling of lithospheric extension, *J. Geophys. Res.*, 97, 2015-2036, 1992.

Dahlen F. A., and T. D. Barr, Brittle frictional mountain building, 1, Deformation and mechanical energy budget, *J. Geophys. Res.*, 94, 3906-3922, 1989.

Davis, D., J. Suppe, and F. A. Dahlen, Mechanics of fold-and-thrust belts and accretionary wedges, *J. Geophys. Res.*, 88, 1153-1172, 1983.

Dunber, J. A., and D. S. Sawyer, How preexisting weaknesses control the style of continental breakup, *J. Geophys. Res.*, 94, 7278-7292, 1989.

England P. C., and G. A. Houseman, Finite strain calculations of continental deformation, 2, Application to the India-Asia collision zone, *J. Geophys. Res.*, 91, 3664-3676, 1986.

England P. C., and G. A. Houseman, Extension during continental convergence, with application to the Tibetan Plateau, *J. Geophys. Res.*, 94, 17,561-17,579, 1989.

England, P. C., and D. P. McKenzie, A thin viscous sheet model for continental deformation, *Geophys. J. R. Astron. Soc.*, 70, 295-321, 1982.

England, P. C., and D. P. McKenzie, Correction to "A thin viscous sheet model for continental deformation", *Geophys. J. R. Astron. Soc.*, 73, 523-532, 1983.

Gill, J. B., *Orogenic Andesites and Plate Tectonics*, Springer-Verlag, New York, 1981.

Goetze, C., The mechanism of creep in olivine, *Philos. Trans. R. Soc. London*, ser. A, 288, 99-119, 1978.

Hamilton, W., Mesozoic California and underflow of Pacific mantle, *Geol. Soc. Am. Bull.*, 80, 2409-2430, 1969.

Houseman, G. A., and P. C. England, Finite strain calculations of continental deformation, 1, Method and general results for convergent zones, *J. Geophys. Res.*, 91, 3651-3663, 1986.

Jischke, C. J., On the dynamics of descending lithospheric plates and slip zones, *J. Geophys. Res.*, 80, 4809-4813, 1975.

Kirby, S. H., and A. K. Kronenberg, Rheology of the lithosphere: Selected topics, *Rev. Geophys.*, 25, 1219-1244, 1987.

Koons, P. O., Some thermal and mechanical consequences of rapid uplift: An example from the Southern Alps, New Zealand, *Earth Planet. Sci. Lett.*, 86, 307-319, 1987.

Lyon-Caen, H., P. Molnar, and G. Suarez, Gravity anomalies and flexure of the Brazilian Shield beneath the Bolivian Andes, *Earth Planet. Sci. Lett.*, 75, 81-92, 1985.

Tao, W., and R. J. O'Connell, Ablative subduction: A two-sided alternative to the conventional subduction theory, *J. Geophys. Res*, 97, 8877-8904, 1992.

Turcotte, D. L. and G. Schubert, *Geodynamics, Application of Continuum Physics to Geological Problems*, John Wiley, New York, 1982.

Turner, J. S., *Buoyancy Effects in Fluids*, Cambridge University Press, New York, 1973.

Vilotte, J. P., M. Daignieres, and R. Madariaga, Numerical modeling of intraplate deformation. Simple mechanical models of continental collision, *J. Geophys. Res.*, 87, 10,709-10,728, 1982.

Vilotte, J. P., M. Daignieres, R. Madariaga, and O. C. Zienkiewicz, Numerical study of continental collision: Influence of buoyancy forces and an initial stiff inclusion, *Geophys. J. R. Astron. Soc.*, 84, 279-310, 1986.

Wdowinski, S., Dynamically supported trench topography, *J. Geophys. Res.*, 97, 17,651-17,656, 1993.

Wdowinski, S., and Y. Bock, The evolution of deformation and topography of high elevated plateaus, 2, Application to the central Andes, *J. Geophys. Res.*, this issue.

Wdowinski, S., and R. J. O'Connell, On the choice of boundary conditions in continuum models of continental deformation, *Geophys. Res. Let.* 17, 2413-2416, 1990.

Wdowinski, S., and R. J. O'Connell, Deformation of the Central Andes (15° 27°S) derived from a flow model of subduction zones, *J. Geophys. Res.*, 96, 12,245-12,255, 1991.

Wdowinski, S., R. J. O'Connell, and P. England, Continuum models of continental deformation above subduction zones: Application to the Andes and the Aegean, *J. Geophys. Res.*, 94, 10,331-10,346, 1989.

Willett, S., C. Beaumont, and P. Fullsack, A mechanical model for the tectonics of doubly-vergent compressional orogens, *Geology*, 21, 371-374, 1993.

Zienkiewicz, O. C., and R. L. Taylor, *The Finite Element Method, vol. 2. Solid and Fluid Mechanics Dynamics and Non-linearity*, 4th ed., McGraw-Hill, New York, 1991.

Y. Bock, Institute of Geophysics and Planetary Physics, Scripps Institution of Oceanography, University of California San Diego, La Jolla, CA 92093-0225. (e-mail: bock@pgga.ucsd.edu)

S. Wdowinski, Geological Survey of Israel, 30 Malkhe Israel St., Jerusalem 95501, Israel. (email: shimon@mail.gsi.gov.il)

(Received November 9, 1992; revised July 13, 1993; accepted August 13, 1993.)